Contactless non-linear optics mediated by long-range Rydberg interactions

Hannes Busche,* Paul Huillery,* Simon W. Ball, Teodora
V. Ilieva, Matthew P. A. Jones, and Charles S. Adams†

Joint Quantum Centre (JQC) Durham-Newcastle,

Department of Physics, Durham University,

South Road, Durham, DH1 3LE, United Kingdom

1

To create effective photon-photon interactions, conventional non-linear optics, linear quantum optics[1,2], cavity quantum electrodynamics (cQED)[3,4], and Rydberg quantum optics[5–10] all employ photons that at one time interacted with matter inside a common medium. Uniquely, Rydberg quantum optics, where optical photons are coherently and reversibly mapped into collective atomic Rydberg excitations[11] gives rise to dipole-mediated effective photon-photon interactions that are long-range[12,13]. Consequently, spatial overlap between light modes is no longer required. We demonstrate a 'contactless' coupling between photons stored as collective Rydberg excitations in spatially separate optical media. The potential induced by each photon modifies the retrieval mode of its neighbour[7,9,14,15] leading to correlations between them. We measure these as a function of interaction strength, distance, and storage time, demonstrating an effective interaction between photons separated by 15 times their wavelength. Contactless effective photon-photon interactions[16] open new perspectives in optics e.g. for scalable multi-channel photonic devices,[15,17] and the study of strongly-correlated many-body dynamics directly using light[18].

In vacuum, photon-photon interactions are so weak that they are only discernible at cosmological scales[19]. This is a remarkable asset for astronomy, imaging, and communications, but a serious obstacle for all-optical processing. In linear quantum optics, one can engineer an effective interaction via measurement[1] which enables entanglement swapping between remote photons[2], however, this relies on probabilistic post-selective measurements. Inside a medium, interactions between light fields are possible, if the light-matter coupling is non-linear. For sufficiently strong non-linearities, as in cQED[3] or Rydberg quantum optics[5], one enters a quantum non-linear regime[20], allowing deterministic effective interactions at the single photon level[4,7–10]. This has paved the way towards proto-typical single-photon transistors[21,22], phase-shifters[23], and photon gates[24].

A unique feature of Rydberg-mediated quantum non-linear optics[5] is that the interaction is long range[12,13], and can be mediated through free space by virtual microwave photons. This adds new geometric degrees of freedom to the non-linear optics tool-box which could facilitate scalable photonic networks, quantum simulation with photons, and circumvent 'no-go' theorems that limit the scope for all-optical quantum information processing (QIP)[15–17,25]. To directly demonstrate the long-range character of Rydberg mediated non-

linear optics, we realise two strongly-interacting photonic channels in independent optical media separated by an adjustable distance d of more than $10\,\mu$m. While stored as collective Rydberg excitations, van der Waals (vdW) interactions imprint non-uniform phase shifts[14,15] that lead to reduced retrieval in the photons' initial modes (figure 1). By counting photons in the unperturbed modes, the reduction is manifest as a spatial anti-correlation in the observed photon statistics. The media can be viewed as two 'black-boxes' which make photons interact at a distance suppressing simultaneous retrieval in both channels.

Consider two weak optical pulses focussed into independent atomic media, labelled A and B, and stored as strongly-interacting collective Rydberg excitations or polaritons[7,9] using electromagnetically induced transparency (EIT, see figure 2a)[26]. During storage, a photon in channel $A(B)$ is coherently converted into the collective atomic excitation

$$|R\rangle_{A(B)} = \frac{1}{\sqrt{\mathcal{N}_{A(B)}}} \sum_{j\in A(B)} e^{i\vec{k}_{A(B)}\vec{r}_j}|R_j\rangle_{A(B)} \ , \tag{1}$$

where $\mathcal{N}_{A(B)}$ is the atom number in the channel, $\vec{k}_{A(B)}$ the wave vector of the EIT light fields, $\vec{r}_j$ the position of atom j, and $|R_j\rangle_{A(B)}$ the collective state where atom j is in Rydberg state $|r\rangle$ with all others in ground state $|g\rangle$. If the individual phases $\vec{k}_{A(B)}\vec{r}_{j(k)}$ in the collective excitation remain unchanged during storage, the phase and spatial mode of the photon are preserved. However, when photons are stored in both channels for a storage time $t_{\rm st}$, the two-channel collective state $|R\rangle_{AB} = |R\rangle_A \otimes |R\rangle_B$ evolves according to

$$\hat{U}(t_{\rm st})_{AB} = \sum_{j\in A, k\in B} e^{-iV_{jk}t_{\rm st}}(|R_j\rangle_A \otimes |R_k\rangle_B)(\langle R_j|_A \otimes \langle R_k|_B). \tag{2}$$

Here, $V_{jk} = n^{11}C_6'/r_{jk}^6$ is the vdW potential, n the principal quantum number of $|r\rangle$, C_6' the reduced vdW coefficient, and $r_{jk} = |\vec{r}_j - \vec{r}_k|$. The spatially dependent interaction-induced phase $V_{jk}t_{\rm st}$ accumulated between atom j in $|R\rangle_A$ and k in $|R\rangle_B$ leads to photon retrieval in different modes than before storage.

In the experiment, see figure 2, we prepare two ensembles of ^{87}Rb atoms in side-by-side optical tweezers separated by a distance $d = 10 - 15\,\mu$m. We focus separate signal pulses, duration $350\,$ns and mean photon number ≈ 2.2, into each ensemble with $1/e^2$ radii of $\approx 1\,\mu$m. The signal photons are resonant with the $|g\rangle = |5S_{1/2}, F = 2, m_F = 2\rangle \rightarrow |e\rangle =$

3

$|5P_{3/2}, F' = 3, m'_F = 3\rangle$ transition as shown in figure 2a. A counter-propagating control field resonantly couples $|e\rangle \rightarrow |r\rangle = |nS_{1/2}\rangle$. Signal and control light have opposing circular polarisation. To store signal photons, the control field is turned off as indicated by the fading blue line in figure 2b.

Subsequently, we retrieve the signal photons by restoring the control field to its original intensity after a time $t_{\mathrm{st}} \approx 170\,\mathrm{ns}$. The photons retrieved in each channel are detected independently by pairs of single-photon detectors (SPADs) arranged in Hanbury-Brown Twiss (HBT) setups. We verify that there is no cross-talk between channels in the storage-retrieval cycle by observing that no photon is retrieved in channel A if only the medium of channel B is present, and vice versa (figure 2b).

We analyse the counting statistics of photons for each channel using the correlation function

$$g_A^{(2)} = \frac{\langle N_A \cdot (N_A - 1)\rangle}{\langle N_A\rangle^2} \ , \tag{3}$$

where N_A is the number of photons retrieved in channel A, similarly for $g_B^{(2)}$. For principal quantum number $n = 80$, interaction-induced dephasing[7,9,14] and Rydberg blockade[27] limit the number of photons stored to close to one per channel as indicated by strong anti-bunching in the single-channel correlation functions, $g_A^{(2)} = 0.17 \pm 0.03$ and $g_B^{(2)} = 0.20 \pm 0.04$. Consequently, the interactions between channels presented below occur at the level of individual photons.

In order to observe a cross-channel interaction, we store photons simultaneously in adjacent channels and analyse the cross-channel correlation function

$$g_{AB}^{(2)} = \frac{\langle N_A \cdot N_B\rangle}{\langle N_A\rangle\langle N_B\rangle} \ . \tag{4}$$

For uncorrelated retrieval one expects $g_{AB}^{(2)} = 1$, whereas $g_{AB}^{(2)} \neq 1$ would indicate an interaction between channels. For $d = 10\,\mu\mathrm{m}$ and $n = 80$, we find $g_{AB}^{(2)} = 0.40 \pm 0.03$ indicating an effective long-range interaction between non-overlapping, spatially separate photons.

To verify that the observed interactions arise from the vdW potential V_{jk}, we vary the interaction strength by changing the principal quantum number n. The data for fixed distance $d = 10\,\mu\mathrm{m}$ and n between 50 and 80 (figure 3a) shows that the interaction between

4

channels increases with n, as expected. Interactions within each channel (inset, figure 3b) also limit the number of photons stored and retrieved. For $n < 65$, we observe no correlations between channels, but intra-channel interactions are still present.

To demonstrate the scaling of the Rydberg mediated interaction with distance, we measure $g_{AB}^{(2)}$ as a function of the channel separation d, for a Rydberg state with $n = 80$ (figure 4a). As d is decreased, one alters the distribution of pair spacings, r_{jk} ($r_{jk} \gtrsim d$ for j, k in adjacent channels) to smaller values leading to stronger interactions. Consequently we observe a change from no correlation, $g_{AB}^{(2)} = 1.0$, at $d = 15\ \mu$m to strong interaction-induced anti-correlations at $d = 10\ \mu$m. As expected, the single channel correlation functions are independent of d (figure 4b). A key implication is the ability to separately tune the on-site and between-site interactions. This is equivalent to a decoupling of self- and cross-Kerr non-linearities[16] which is not possible in conventional non-linear media and has the potential to become a major resource for non-linear optics, e.g. in optical QIP[15,17,25].

To compare our results to theory, we extend previous theoretical work[14] on interaction-induced dephasing within a single channel to model the effect of phase shifts in our dual-channel geometry (dashed lines in figures 3, 4, and 5, see Methods for more details). Spatial averaging of the phase-shifts over all atoms contributing to the collective states means that interaction falls off more slowly than for the individual pair-wise terms, V_{jk}. We also verified that anti-correlations increase with the storage time t_{st} (figure 5) as expected because the interaction induced phase scales as $V_{jk}t_{\mathrm{st}}$. This and the good agreement between theory and experiment when we vary the interaction strength (figure 3) or distance (figure 4) indicates that interaction-induced phase shifts make an important contribution to the overall interaction. While the channels are separated by more than the radius, $r_{\mathrm{b}}(80S_{1/2}) \approx 9\ \mu\mathrm{m} < d$, for inter-channel dipole blockade between collective excitations[11,27], blockade effects beyond d associated with the storage protocol[18] may also contribute to the interaction.

Rydberg mediated long-range interactions between spatially separated optical photons are a novel and powerful addition to optics. If tailored to imprint uniform phase shifts, the micron-scale interaction length provides a convenient starting point for scalable all-optical QIP[15,17] based on tweezer arrays[28] or coupled to optical circuits in integrated photonic waveguides[29]. Quantum simulators based on dipolar interactions, e.g. of spin models[30] or non-radiative energy transfer[31], may now be realised with photons stored as collective Rydberg excitations providing the added benefit of fast coherent read-out and the ability to

measure both amplitude and phase.

METHODS

Experimental setup and preparation of atomic media. Each photonic channel consists of a tightly-focussed signal beam and a microscopic optical tweezer confining cold atoms. This requires near diffraction limited optical resolution. We achieve this using a pair of aspheric lenses (numerical aperture ≈ 0.5, focal length $\approx 10\,\text{mm}$) placed inside the ultra-high vacuum chamber in which experiments take place. As Rydberg atoms are highly sensitive to electric fields, conductive transparent indium-tin-oxide coatings have been applied to the dielectric lens surfaces facing the atoms to avoid charge build-up in their vicinity. A detailed description of the experimental setup can be found elsewhere[32].

The experimental procedure is as follows. Initially we trap atoms in a magneto-optical trap (MOT) which is loaded from a cold bright atomic beam created by a 2D MOT in $100\,\text{ms}$. Subsequently, we increase their density and decrease their temperature by first compressing the MOT via an increase in the magnetic field gradient and then subjecting them to a grey optical molasses phase. The red-detuned dipole trap beams at a wavelength of $910\,\text{nm}$ are focussed to $1/e^2$ radii of $\approx 4.5\,\mu\text{m}$ creating traps with depths of $\approx 400\,\mu\text{K}$, and are turned on right from the start of the MOT loading. Once the MOT is switched off, we apply free evaporative cooling for $400\,\text{ms}$ which reduces the volume of the trapped atoms to avoid any overlap between signal beam A and medium B, or vice versa. The resulting two cigar shaped clouds with estimated radii (standard deviations of Gaussian atom distribution) $\approx 20\,\mu\text{m}$ (axial) and $\approx 1.5\,\mu\text{m}$ (radial), contain on the order of $\propto 10^3$ atoms each. These estimates are based on upper bounds obtained from imaging and the calculated trapping potentials. They are consistent with our observation that the absorption is reduced if the signal beam waist exceeds $2\,\mu\text{m}$, and with the values obtained from fitting the dephasing model as described below.

The signal beams are overlapped with the respective trapping beams for each channel to simplify adjusting the distance d between channels by enabling simultaneous alignment of both beams. The channel separation is measured and adjusted by imaging the signal foci at approximately 39 fold magnification. Besides verifying the absence of cross-talk in photon storage as shown in figure 2, we also verify that there is no significant cross-talk in the

6

absorption of the signal light providing stronger evidence of no overlap between channels. While we observe $2 - 3\%$ cross-absorption for $d = 10\,\mu$m, it vanishes for $d_{AB} \geq 11\,\mu$m (see figure in supplementary information), well below the threshold where the photon retrieval becomes uncorrelated between channels as $g^{(2)}_{AB}$ approaches 1 (see figure 4a).

Photon storage. Following the preparation of the atom clouds, we optically pump the atoms to the state $|g\rangle = |5S_{1/2}, F = 2, m_F = 2\rangle$. Subsequently, the trapping light is turned off for $1.5\,\mu$s, every $4.55\,\mu$s during which we carry out one storage and retrieval sequence as shown in figure 2b. Since heating of the ensemble and atom loss are low due to the weak signal pulse, we can repeat this sequence $25,000$ times before reloading the traps. This corresponds to an effective cycle rate of $33.5\,$kHz, mostly determined by the time needed to prepare the atomic ensembles, i.e. loading of the MOT and evaporation. In total, we repeat the storage and retrieval sequence 25 million times for each datapoint presented, except for the data in figure 5 where up to 156 million repetitions are carried out due to lower retrieval at longer storage times. The initial Rabi frequency of the control field is $\Omega_{\mathrm{C}}/2\pi \approx 9\,$MHz for the data in figure 3 and $\approx 7\,$MHz for figures 4 (except for $d = 10\,\mu$m where $\Omega_{\mathrm{C}}/2\pi \approx 9\,$MHz) and 5. The storage times t_{st} excludes the fall and rise time of the control field.

The overall efficiencies for the photon storage/retrieval protocol in these experiments are typically between 1 to 3%, limited by strong interactions within the same channel and the small cloud size and thus limited optical depth of the atomic media[33]. Working at weaker signal pulses with mean photon number well below 1 and using slightly larger atom clouds, we have previously achieved efficiencies on the order of $\approx 10\%$, while the current published record for storage in Rydberg states stands at $\approx 20\%$[23]. Increasing the optical depth by increasing the atomic density proves difficult, as additional dephasing occurs due to interactions between ground state atoms and Rydberg electrons if the inter-atomic spacing becomes equivalent to the size of the electron orbit[34], though this might not be problematic when engineering dissipative interactions[33]. Recently, ordered atomic monolayers have been suggested as a promising alternative to achieve high optical depth at well controlled inter-atomic spacings[35].

Single-photon detection and correlation analysis. The signal light retrieved in the unperturbed modes is coupled into polarisation maintaining single mode fibres to filter out stray light and spontaneous emission from the decay of dephased polaritons. The 50:50 beam splitters for HBT interferometry are located behind the fibres. We record all detection events

independently for each detector using a home-built FPGA system with a timing resolution of 5 ns. The detection efficiencies of signal photons emitted from the atomic ensembles are typically 20 % for channel A and 21 % for channel B, including all loss on subsequent optical elements, i.e. transmission loss on the indium-tin oxide coating on the in-vacuum lens, laser line filters, and finite coupling efficiencies into the single-mode fibres, as well as the quantum efficiencies of the SPADs.

To evaluate the correlation functions given in the main text, we analyse the photon statistics in software post-processing based on the recorded timestamps of detection events. Due to the finite dead-time of the SPADs, we limit our analysis of photon numbers to as many detection events as detectors, i.e. two per channel, within the retrieval window. We account for imbalances in the 50:50 HBT splitting ratio resulting from imperfect beam-splitters and imbalanced detection efficiencies.

Formal description of the interaction-induced phase shift mechanism and simulations of retrieved photon statistics. In the following, we describe the mechanism that gives rise to the phase-shift in detail and simulate the effect on the retrieved photon statistics. We build upon work by Bariani *et al.*[14] who describe interaction-induced dephasing between collective Rydberg excitations within a single atomic ensemble. We expand their work to include multiple, arbitrarily shaped signal modes and atomic media to simulate the two-channel geometry of our experiment. We consider the following two scenarios: a single channel containing no more than two excitations in the same medium; and a pair of spatially separated channels containing no more than a single excitation per channel. The truncation to two excitations is justified since in comparison, triple excitations are highly unlikely due to the low number of photons which is retrieved per storage cycle (on the order of a few 0.01). Despite its simplicity, this approach allows for full exploration of the mechanism and successfully reproduces experimental data.

Initially, we consider storage in the same channel (here labelled A). Starting from the atomic ensemble's collective ground state $|G\rangle_A$, storage of ν photons results in the collectively excited state $|R^{(\nu)}\rangle_A = (\hat{S}_A^\dagger)^\nu |G\rangle_A / \sqrt{\nu!}$ where

$$\hat{S}_A^\dagger = \frac{1}{\sqrt{\sum_j \epsilon_A(\vec{r}_j)^2}} \sum_j \epsilon_A(\vec{r}_j) e^{i\varphi_A(\vec{r}_j)} |r\rangle_{j,A} \langle g|_{j,A} \qquad (5)$$

describes the creation of an (additional) collective excitation. Here, $|g\rangle_{j,A}$ and $|r\rangle_{j,A}$ cor-

8

respond to the ground and Rydberg states of atom j, $\epsilon_A(\vec{r}_j)$ and $\varphi_A(\vec{r}_j)$ are respectively the electric field amplitude of the signal mode and the combined phase of both EIT fields at the position $\vec{r}_j$ of atom j. We preserve approximately correct normalisation in the limit $\nu \ll \mathcal{N}_A$. We consider the atomic ensemble of a single channel to be in a superposition $|R\rangle_A = \sum_{\nu \leq 2} c_\nu |R^{(\nu)}\rangle_A$ following storage where the coefficients c_ν describe the distribution between excitation numbers neglecting more than two excitations as explained above.

In the presence of van-der-Waals interactions described by $V_{jk} = n^{11} C_6' / r_{jk}^6$, the individual Rydberg excitation pairs contributing to $|R^{(2)}\rangle_A$ evolve during t_{st} according to

$$\hat{U}_{(A)}(t_{\mathrm{st}}) = \sum_{j,k>j} e^{-iV_{jk}t_{\mathrm{st}}} |R_{j,k}\rangle_A \langle R_{j,k}|_A \tag{6}$$

where $|R_{j,k}\rangle_A$ corresponds to the collective state where atoms j and k are excited. Since the phase shifts $V_{jk}t_{\mathrm{st}}$ acquired between pairs vary with position, the collective state dephases as a consequence of the interactions thus reducing the probability to retrieve both photons in the original signal mode from $\hat{U}_A(t_{\mathrm{st}})|R^{(2)}\rangle_A$. The overlap

$$\begin{aligned}
D_A &= \frac{\langle G|_A \hat{S}_A^2 \hat{U}_A(t_{\mathrm{st}})(\hat{S}_A^\dagger)^2 |G\rangle_A}{\langle G|_A \hat{S}_A^2 (\hat{S}_A^\dagger)^2 |G\rangle_A} \\
&= \frac{\sum_{j,k>j} (\epsilon_A(\vec{r}_j)\epsilon_A(\vec{r}_k))^2 e^{-iV_{jk}t_{\mathrm{st}}}}{\sum_{j,k>j} (\epsilon_A(\vec{r}_j)\epsilon_A(\vec{r}_k))^2}
\end{aligned} \tag{7}$$

between $|G\rangle_A$ and the collective state of the ensemble after retrieval of two photons in the signal mode from the time-evolved doubly excited state quantifies the dephasing, and allows us to compare the experimentally measured correlation function $g_A^{(2)}$ to theory via

$$g_A^{(2)} = \frac{2|D_A|^2 |c_2|^2}{(|c_1|^2 + 2|D_A|^2 |c_2|^2)^2}. \tag{8}$$

Building on the single channel case, we quantify interactions between photons stored as collective Rydberg excitations in two adjacent, non-overlapping channels. For two channels A and B, the initial state with exactly ν (μ) Rydberg excitations in channels $A(B)$ after photon storage, can be written as product $|R^{(\nu,\mu)}\rangle_{AB} = |R^{(\nu)}\rangle_A \otimes |R^{(\mu)}\rangle_B$ of the individual single channel states. Hence, the collective state of both channels immediately after storage is $|R\rangle_{AB} = \sum_{\nu,\mu \in \{0,1\}} c_{\nu,\mu} |R_{AB}^{(\nu,\mu)}\rangle$ where $c_{\nu,\mu}$ again arise from the photon number distributions

of the original signal pulses. Evolving over t_{st}, the individual excitation pairs in $|R^{(1,1)}\rangle_{AB}$ again acquire non-uniform interaction-induced phases as

$$\hat{U}(t_{st})_{AB} = \sum_{j \in A, k \in B} e^{-iV_{jk}t_{st}} (|R_j\rangle_A \otimes |R_k\rangle_B)(\langle R_j|_A \otimes \langle R_k|_B). \tag{9}$$

To estimate the effect of the imprinted phase shifts on the retrieved photon statistics, we now consider the overlap

$$D_{AB} = \frac{\langle G|_{AB} \hat{S}_A \hat{S}_B \hat{U}_{AB}(t_{st}) \hat{S}_A^\dagger \hat{S}_B^\dagger |G\rangle_{AB}}{\langle G|_{AB} \hat{S}_A \hat{S}_B \hat{S}_A^\dagger \hat{S}_B^\dagger |G\rangle_{AB}} \tag{10}$$

where $|G\rangle_{AB} = |G\rangle_A \otimes |G\rangle_B$ and obtain

$$g_{AB}^{(2)} = \frac{|D_{AB}|^2 |c_{1,1}|^2}{(|c_{1,0}|^2 + |D_{AB}|^2 |c_{1,1}|^2)(|c_{0,1}|^2 + |D_{AB}|^2 |c_{1,1}|^2)}. \tag{11}$$

To compare experimental results to theory, we calculate both cross- and single channel correlation functions as above based on the experimental parameters described at the beginning of the Methods, assuming $\mathcal{N}_{A(B)} = 1000$ atoms per trap. The numbers of photons stored in each channel follow a Poissonian distribution with mean $\overline{\nu}, \overline{\mu} = 0.01$, with no initial correlation between channels and neglecting blockade[27] effects: $|c_\nu|^2 = e^{-\overline{\nu}} \overline{\nu}^\nu / \nu!$ and $|c_{\nu,\mu}|^2 = |c_\nu|^2 |c_\mu|^2$. By varying both $\mathcal{N}_{A(B)}$ and $\overline{\nu}(\overline{\nu})$, we verify that their values do not impact the results provided that the condition $\overline{\nu}(\overline{\mu}) \ll 1 \ll \mathcal{N}_{A(B)}$ is met. The storage time is $t_{st} = 170\,\text{ns}$ (except for simulations in figure 5) and the interaction strength of V_{jk} is set based on the Rydberg state considered. The simulation results are averaged over 10 different instances for the atom distributions per datapoint. Although the model does not include any free parameter itself, t_{st} and the atom cloud sizes are not precisely experimentally verifiable (see above), and we use them as adjustable parameters.

AUTHOR CONTRIBUTIONS

All authors contributed to the experiment, analysis and discussion of the results, as well as the preparation of the manuscript.

AUTHOR INFORMATION

The authors declare no competing financial interests. Correspondence and requests for materials should be addressed to C. S. A. (c.s.adams@durham.ac.uk).

DATA AVAILABILITY

The data presented in this letter are available at `http://dx.doi.org/doi:10.15128/r1wh246s12j`.

---

* These authors contributed equally to this work.

† c.s.adams@durham.ac.uk

[1] Knill, E., Laflamme, R., and Milburn, G. J. A scheme for efficient quantum computation with linear optics. Nature **409**, 46–52 (2001).

[2] Pan, J.-W., Bouwmeester, D., Weinfurter, H. and Zeilinger, A. Experimental Entanglement Swapping: Entangling Photons That Never Interacted. Phys, Rev. Lett. **80**, 3891–3894 (1998).

[3] Reiserer, A. and Rempe, G. Cavity-based quantum networks with single atoms and optical photons. Rev. Mod. Phys. **87**, 1379–1418 (2015).

[4] Birnbaum, K. M. *et al.* Photon blockade in an optical cavity with one trapped atom. Nature **436**, 87–90 (2005).

11

[5] Firstenberg, O., Adams, C. S., and Hofferberth, S. Nonlinear quantum optics mediated by Rydberg interactions. J. Phys. B: At. Mol. Opt. Phys. **49**, 152003 (2016).

[6] Pritchard, J. D. *et al.* Cooperative Atom-Light Interaction in a Blockaded Rydberg Ensemble. Phys. Rev. Lett. **105**, 193603 (2010).

[7] Dudin, Y. O. and Kuzmich, A. Strongly Interacting Rydberg Excitations of a Cold Atomic Gas. Science **336**, 887–889 (2012).

[8] Peyronel, T. *et al.* Quantum nonlinear optics with single photons enabled by strongly interacting atoms. Nature **448**, 57–60 (2012).

[9] Maxwell, D. *et al.* Storage and Control of Optical Photons Using Rydberg Polaritons. Phys. Rev. Lett. **110**, 103001 (2013).

[10] Firstenberg, O. *et al.* Attractive Photons in a Quantum Nonlinear Medium. Nature **502**, 71–75 (2013).

[11] Ebert, M., Kwon, M., Walker, T. G., and Saffman M. Coherence and Rydberg Blockade of Atomic Ensemble Qubits. Phys. Rev. Lett. **115**, 093601 (2015).

[12] Gorshkov, A. V., Otterbach, J., Fleischhauer, M., Pohl, T., and Lukin, M. D. Photon-Photon Interactions via Rydberg Blockade. Phys. Rev. Lett. **107**, 133602 (2011).

[13] Sevinçli, S., Henkel, N., Ates, C., and Pohl, T. Nonlocal Nonlinear Optics in Cold Rydberg Gases. Phys. Rev. Lett. **107**, 153001 (2011).

[14] Bariani, F., Goldbart, P. M., and Kennedy, T. A. B. Dephasing dynamics of Rydberg atom spin waves. Phys. Rev. A **86**, 041802(R) (2012).

[15] Khazali, M., Heshami, K., and Simon, C. Photon-photon gate via the interaction between two collective Rydberg excitations. Phys. Rev. A **91**, 030301(R) (2015).

[16] He, B. Sharypov, A. V., Sheng, J., Simon, C., and Xiao, M. Two-Photon Dynamics in Coherent Rydberg Atomic Ensemble. Phys. Rev. Lett. **112**, 133606 (2014).

[17] Paredes-Barato, D. and Adams, C. S. All-Optical Quantum Information Processing Using Rydberg Gates. Phys. Rev. Lett. **112**, 040501 (2014).

[18] Moos, M., Höning, M., Unanyan, R., and Fleischhauer, M. Many-body physics of Rydberg dark-state polaritons in the strongly interacting regime. Phys. Rev. A **92**, 053846 (2015).

[19] Heisenberg, W. and Euler, H. Folgerungen aus der Diracschen Theorie des Positrons. Z. Phys. **98**, 714–732 (1936).

[20] Chang, D. E., Vuletić, V., and Lukin, M.D. Quantum nonlinear optics - photon by photon. Nat. Photon. **8**, 685–694 (2014).

[21] Gorniaczyk, H., Tresp, C., Schmidt, J., Fedder, H., and Hofferberth, S. Single-Photon Transistor Mediated by Interstate Rydberg Interactions. Phys. Rev. Lett. **113**, 053601 (2014).

[22] Tiarks, D., Baur, S., Schneider, K., Dürr, S., and Rempe, G. Single-Photon Transistor Using a Förster Resonance. Phys. Rev. Lett. **113**, 053602 (2014).

[23] Tiarks, D., Schmidt, S., Rempe, G., and Dürr, S. Optical π phase shift created with a single-photon pulse. Sci. Adv. **2**, 160036 (2016).

[24] Hacker, B., Welte, S., Rempe, G., and Ritter, S. A photon–photon quantum gate based on a single atom in an optical resonator. Nature **536**, 193–196 (2016).

[25] Shapiro, H. Single-photon Kerr nonlinearities do not help quantum computation. Phys. Rev. A **73**, 062305 (2006).

[26] Fleischhauer, M. and Lukin, M. D. Dark-State Polaritons in Electromagnetically Induced Transparency. Phys. Rev. Lett. **84**, 5094–5097 (2000).

[27] Lukin, M.D. *et al.* Dipole Blockade and Quantum Information Processing in Mesoscopic Atomic Ensembles. Phys. Rev. Lett. **87**, 037901 (2001).

[28] Nogrette, F., *et al.* Single-Atom Trapping in Holographic 2D Arrays of Microtraps with Arbitrary Geometries. Phys. Rev. X **4**, 021034 (2014).

[29] Kohnen, M. *et al.* An array of integrated atom-photon junctions. Nat. Photon. **5**, 35–38 (2011).

[30] Barredo, D. *et al.* Coherent Excitation Transfer in a Spin Chain of Three Rydberg Atoms. Phys. Rev. Lett. **114**, 113002 (2015).

[31] Günter, G. *et al.* Observing the Dynamics of Dipole-Mediated Energy Transport by Interaction-Enhanced Imaging. Science **342**, 954–956 (2013).

[32] Busche, H., Ball, S. W., and Huillery, P. A high repetition rate experimental setup for quantum non-linear optics with cold Rydberg atoms. Eur. Phys. J. Special Topics, 225, 2839–2861 (2016).

[33] Gorshkov, A. V., Nath, R. and Pohl, T. Dissipative Many-Body Quantum Optics in Rydberg Media. Phys. Rev. Lett. **110**, 153601 (2013).

[34] Gaj, A. *et al.* From molecular spectra to a density shift in dense Rydberg gases. Nat. Commun. **5**, 4546 (2014).

[35] Bettles, R. J., Gardiner, S. A., and Adams, C. S. Enhanced Optical Cross Section via Collective Coupling of Atomic Dipoles in a 2D Array. Phys. Rev. Lett. **116**, 103602 (2016).
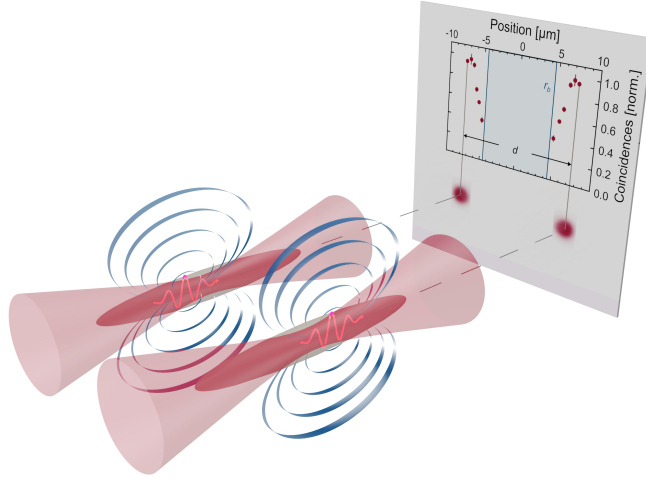
Figure 1. Contactless interactions between photons stored as collective Rydberg excitations in spatially separated channels. Each channel consists of an optical mode tightly focussed inside a microscopic cloud of ultra-cold atoms where signal photons are stored and retrieved. When two photons are stored in both channels simultaneously, vdW-interactions induce spatially dependent phase shifts which modify the retrieval modes. The reduction in the coincidence count rate as the two channels are moved closer together is shown on the screen. Strong cross-channel interaction effects appear at a separation $d = 12\,\mu$m which is both larger than the blockade radius r_b for individual Rydberg atoms at $|80S_{1/2}\rangle$ and equal to 15 times the optical wavelength.
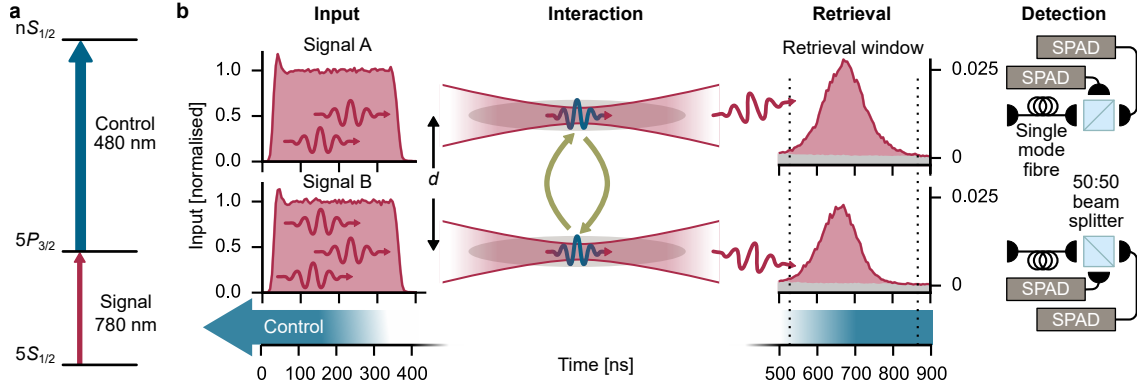
Figure 2. Experimental realisation. a, Transitions in ^{87}Rb used for EIT-based photon storage. Signal photons: $|g\rangle = |5S_{1/2}, F = 2, m_F = 2\rangle \rightarrow |e\rangle = |5P_{3/2}, F' = 3, m'_F = 3\rangle$, control field: $|e\rangle \rightarrow |r\rangle = |nS_{1/2}\rangle$. **b,** Photon storage procedure. While signal pulses propagate through the media, the common control field is switched off. For retrieval, it is restored to its original value. The counting statistics of the retrieved signal photons are analysed using SPADs in two HBT setups. The actual input and retrieved signal pulses are shown. The cross-talk is zero as no retrieved photons above dark count (grey) are detected in channel B when only storage medium A is present, and vice versa.
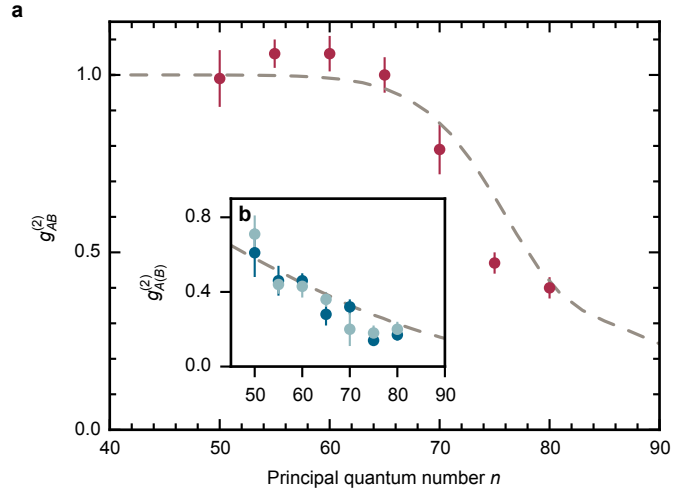
Figure 3. Effect of interaction strength on retrieved photon statistics for channel separation $d = 10\,\mu$m **and** $t_{\mathrm{st}} = 170$ **ns. a,** Cross-channel correlation function $g_{AB}^{(2)}$ measured for photon retrieval after storage in Rydberg states with principal quantum number n. As the interaction strength increases as n^{11}, an interaction between channels $g_{AB}^{(2)} < 1$ is only observed for $n > 65$. **b,** Single channel correlation functions $g_{A(B)}^{(2)}$ in absence of the other channel (A: light, B: dark blue). The grey dashed lines are the expected results based on simulations (see text). Errorbars correspond to statistical standard errors.
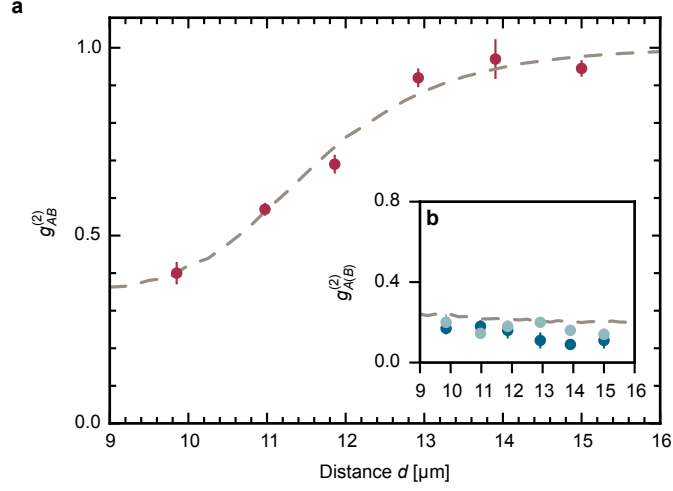
Figure 4. Effect of channel separation d on retrieved photon statistics for principal quantum number $n = 80$ and $t_{\mathrm{st}} = 170$ ns. a, Cross-channel correlation function $g_{AB}^{(2)}$ measured for photon retrieval after storage at different channels separations d. **b,** Single channel correlation functions $g_{A(B)}^{(2)}$ in the absence of the other channel (A: light, B: dark blue). The change in $g_{AB}^{(2)}$ while the single channel values $g_{A(B)}^{(2)}$ remain approximately constant as expected, shows that inter-channel interactions can be independently tuned by adjusting d. The grey dashed lines show simulation results. Errorbars correspond to statistical standard errors.
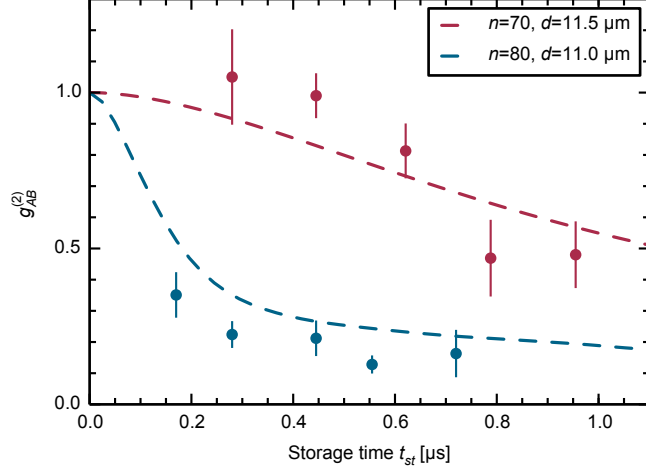
Figure 5. Effect of the storage time t_{st} on retrieved photon statistics. Cross-channel correlation function $g_{AB}^{(2)}$ measured for photon retrieval after storage for a time t_{st} for principal quantum number $n = 70$ and 80 and channel separation $d = 11.5$ μm and 11.0 μm, respectively. The dashed lines show simulation results. Errorbars correspond to statistical standard errors. The maximum storage time is limited by the finite temperature of the atomic ensemble which leads to motional dephasing. Note that the evaporative cooling stage (Methods) employed in all other experiments is omitted resulting in slightly larger atomic media and the observation of cross-talk in signal absorption at $d = 11.5\,\mu$m. No cross-talk is observed in photon storage.
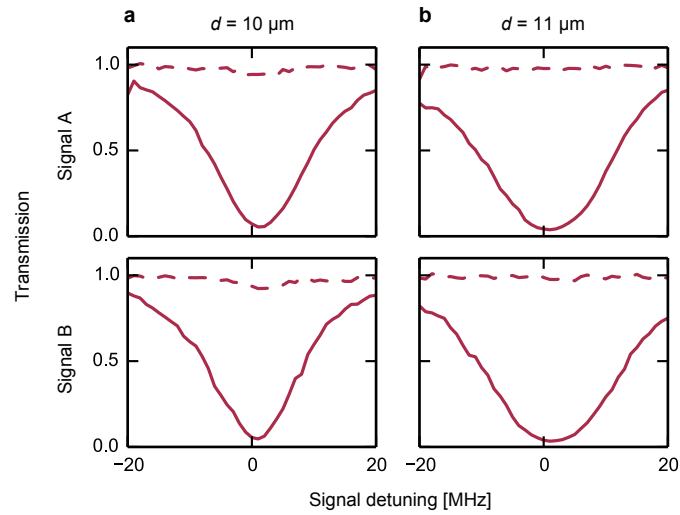
Supplementary figure. Cross-talk in signal absorption between channels. a, Absorprtion spectra for channels A (top) and B (bottom) separated by $d = 10\,\mu$m when both storage media (solid line) or only the medium of the other channel (dashed line) are present. For $d = 10\,\mu$m, we typically observe $2-3\,\%$ cross-absorption. **b,** For separations of $d = 11\,\mu$m as shown here, and greater, we typically observe no cross-talk.